A Review of Interactions Between Ceria and H_2 and their Applications to Selective Hydrogenation of Alkynes

James Kammert,[✝] Jisue Moon,[✝] and Zili Wu*

Chemical Science Division and Center for Nanophase Materials Sciences, Oak Ridge National Laboratory, Oak Ridge, Tennessee 37831, USA.

* Corresponding author: wuz1@ornl.gov (ZW)

[✝] equal contribution

Abstract

Cerium oxide (ceria) has found a wide variety of applications in catalysis including as a catalyst, a modifier, or a support, largely thanks to its robust redox properties and versatile acid-base function. While it is often utilized for oxidation reactions, ceria has recently attracted intense research interest for its unusual ability to selectively hydrogenate alkynes to alkenes. The intriguing hydrogenation ability of ceria has sparked renewed research efforts to understand how pure ceria works as a hydrogenation catalyst. In this review, recent advances in both experimental and computational studies of ceria are summarized, focusing on the interaction of ceria with H_2 and in hydrogenation reactions. Significant insights from various studies including *in situ* spectroscopy/microscopy and theoretic modeling of ceria in hydrogen-involved reactions are discussed, which shed light on the origin of the hydrogenation ability of ceria and the reaction mechanisms involved in ceria-catalyzed alkyne hydrogenation. Ways to further improve both the mechanistic understanding and catalytic performance of ceria-based materials for hydrogenation reactions are proposed at the end in the summary and outlook section.

Key Words: ceria, redox, hydrogen, hydrogenation, hydride, mechanism

1 INTRODUCTION

Cerium oxide (CeO_2, Ceria) finds many applications in catalysis as both a catalyst itself, and as a catalyst support. The first and the most well-known catalytic application of ceria is its use as an oxygen storage component in automotive three-way catalysts (TWC), which convert the main pollutants present in vehicle emissions (CO, NO and unburned hydrocarbons) into less harmful compounds[1]. Over the past few decades, ceria and ceria-based materials have found increasing applications in catalysis thanks to their unique structural and electronic properties. The interesting properties of ceria are associated with its ability to cycle between Ce(III) and Ce(IV) states upon interaction with reducing or oxidizing components in reacting mixtures, forming and annihilating oxygen vacancies in a stable fluorite-type structure[2]. Additionally, ceria is characterized by several types of surface and subsurface defects, which can be controlled by adjusting the surface morphology of the ceria itself, or doping the ceria with other promoters, to form Ce^{3+} species that may form active sites for heterogeneous catalysis[3-7] Ceria also has controllable acid-base properties in the form of both Lewis acid and base sites, depending on ceria morphology and pre-treatment procedures[3, 8, 9] and can efficiently catalyze various organic reactions in both gas phase and aqueous phase.[3, 10-13]

In addition to its redox and acid-base properties, ceria combined with metals has attracted increasing interest in heterogeneous catalysis for various hydrogenation reactions such as H_2 generation[14-16], CO_2 hydrogenation[17-21], and the hydrogenation of different functional groups[22-27]. Recently, pure ceria demonstrated surprising catalytic ability in hydrogenation reactions,[28-31] particularly the selective hydrogenation of alkynes to alkenes in both gas and liquid phases with high selectivity (80-90%).[26, 31, 32] Contrary to observed trends for many redox reactions catalyzed by ceria, the formation of surface oxygen vacancies prior to or during reaction was found detrimental to the hydrogenation activity.[26, 31, 32] Other recent studies[29, 30, 33] showed that oxygen-vacancy-associated frustrated Lewis pairs (FLPs) promoted the hydrogenation of alkynes over porous ceria rods. The hydrogenation ability of bare ceria, without any metallic promoter, has prompted a renewed strong interest in understanding how ceria dissociates H_2 and catalyzes selective hydrogenation, and has been studied using a number of experimental and computational approaches.[22, 23, 25, 33-38]

Many detailed reviews have been written that summarize aspects of ceria or ceria-based materials[3, 4, 8, 30, 39-52], and focus on topics such as redox properties, general oxidation catalysis, and emerging applications including photocatalysis and biomedical technology. There are very limited perspectives[30, 31], however, on hydrogenation reactions catalyzed by ceria-based oxides, and we find no overview focused only on ceria-based materials for hydrogenation without the assistance of a metal component. Therefore, the goal of the present review is to survey the existing understanding of the specific properties of ceria associated with interaction with H_2 and under conditions used for hydrogenation reactions to provide an in-depth understanding of how ceria-based oxides catalyze hydrogenation reactions as well as redox reactions (since reduction of ceria is part of the redox process). We will focus on analyzing experimental and theoretical studies on (1) hydrogen interaction and (2) selective alkyne hydrogenation. Although the focal point is ceria, some relevant cases over doped ceria will also be reviewed. First, we will discuss the experimental aspect concerning the mechanistic understanding and catalytic properties of ceria in interacting with H_2 and selective alkyne hydrogenation. The reductive behaviors of CeO_2 by H_2 and the relation to hydrogenation reactions have been studied in great details by different techniques and the use of these approaches will be surveyed including Fourier transform infrared spectroscopy (FT-IR, DRIFTS)[8, 23, 53], Raman spectroscopy[54], ^{17}O-NMR[55], X-ray photoelectron spectroscopy (XPS)[56, 57], X-ray diffraction[58], and neutron vibrational spectroscopy[38, 53, 59]. After discussing these experimental investigations of ceria, the representative theoretical studies will be reviewed to understand the H_2 dissociation and subsequent hydrogenation mechanisms over ceria at atomic scale. Finally, a summary with the outlook of ceria-based catalysts for hydrogenation reactions is presented.

2 INTERACTION OF H_2 WITH CERIA

2.1 TEMPERATURE-PROGRAMMED REDUCTION AND DESORPTION USING H_2

One of the most straightforward experiments that can be performed to observe the interaction of H_2 with CeO_2 is to heat CeO_2 at a controlled rate under an atmosphere containing H_2. Despite the simplicity of the technique, careful analysis of products or consumption of reactants measured in the effluent using mass spectrometry or thermal conductivity can provide some insight into the dynamic processes that are occurring on the CeO_2 surface as well as in the bulk of the material. The so-called temperature-programmed reduction by H_2 (H_2-TPR) has become a ubiquitous technique used to characterize the surface and bulk properties of CeO_2.[2, 25, 60-68]

The characteristic H_2-TPR profile of CeO_2 generally consists of two main H_2 consumption features near 770 and 1100 K. Consumption of H_2 occurring around 770 K has been ascribed to the reduction of surface oxygen species (forming O vacancies), as the total consumption in this region is well-correlated with the surface area of polycrystalline CeO_2 samples.[2] Consumption of H_2 around 1100 K was ascribed to the reduction of bulk CeO_2, resulting from diffusion of O out of the CeO_2 bulk to the CeO_2 surface where it can react with adsorbed or gas phase H species. Johnson and Mooi proposed a relationship between the total H_2 consumption around 770 K and CeO_2 surface area in CeO_2 samples up to 27 m^2 g^{-1}.[60] Perrichon et al. and Bruce et al. demonstrated that the total consumption of H_2 in this region remains well-correlated with the BET surface area of carbonate-free CeO_2 in samples up to 168 m^2 g^{-1}, although there exists some disagreement between these results and those reported by Johnson and Mooi.[61, 62] Giordano et al. developed a model to describe temperature-programmed consumption of H_2 by CeO_2 with initial surface area up to 44 m^2 g^{-1}, and concluded that the nuances of surface reduction kinetics were still not fully understood.[63] Further consideration of the kinetics of morphological changes in the material (e.g., the sintering of high-surface-area particles) was also deemed critical to understanding the H_2-TPR behavior of CeO_2.[64] As oxygen diffusion in the CeO_2 lattice is expected to be rapid under the conditions required for reduction, the role of different exposed surface planes of CeO_2 was expected to play a significant role in the reduction behavior in the lower-temperature reduction regime.

Indeed, exploration of the role of exposed surface facets using ceria nanoshapes of different morphologies revealed differences in reduction behavior.[65-67] Tana et al. found highly faceted nanoparticles demonstrated a lower oxygen storage capacity than nanorods and nanowires as measured by oxygen titration after reduction.[65] Reversible oxygen storage was attributed to preferential exposure of the (110) surface in rod- and wire-shaped nano-CeO_2 over the less reactive (111) surface exposed on the faceted nanoparticles. Liu et al. observed that surface oxygen was removed by H_2 at lower temperatures as lattice strain was increased, and suggested that catalytic oxidation activity was associated with the reversible oxygen storage capacity of the materials.[66] When Désauney et al. synthesized highly controlled CeO_2 nanocubes, nanorods, and nanooctahedra, a significant difference was observed between the reducibility of the preferentially exposed surface planes.[67] As shown in **Figure 1**, the majority of H_2 consumption observed in the H_2-TPR profiles of CeO_2 nanocubes and nanooctahedra took place above 773 K, while H_2

consumption over the nanorods was split more evenly between temperature regimes around 700 and 950 K. Consumption of H_2 resulting from surface reduction occurred at lower temperatures over nanocubes and nanorods than over the nanooctahedra. Reported apparent activation barriers for surface reduction were 70, 130, and 150 kJ mol^{-1} over nanocubes, nanorods, and nanooctahedra, respectively, corroborating that the ease of reducibility of CeO_2 surface planes follows the trend (100) > (110) > (111), in agreement with Tana et al.

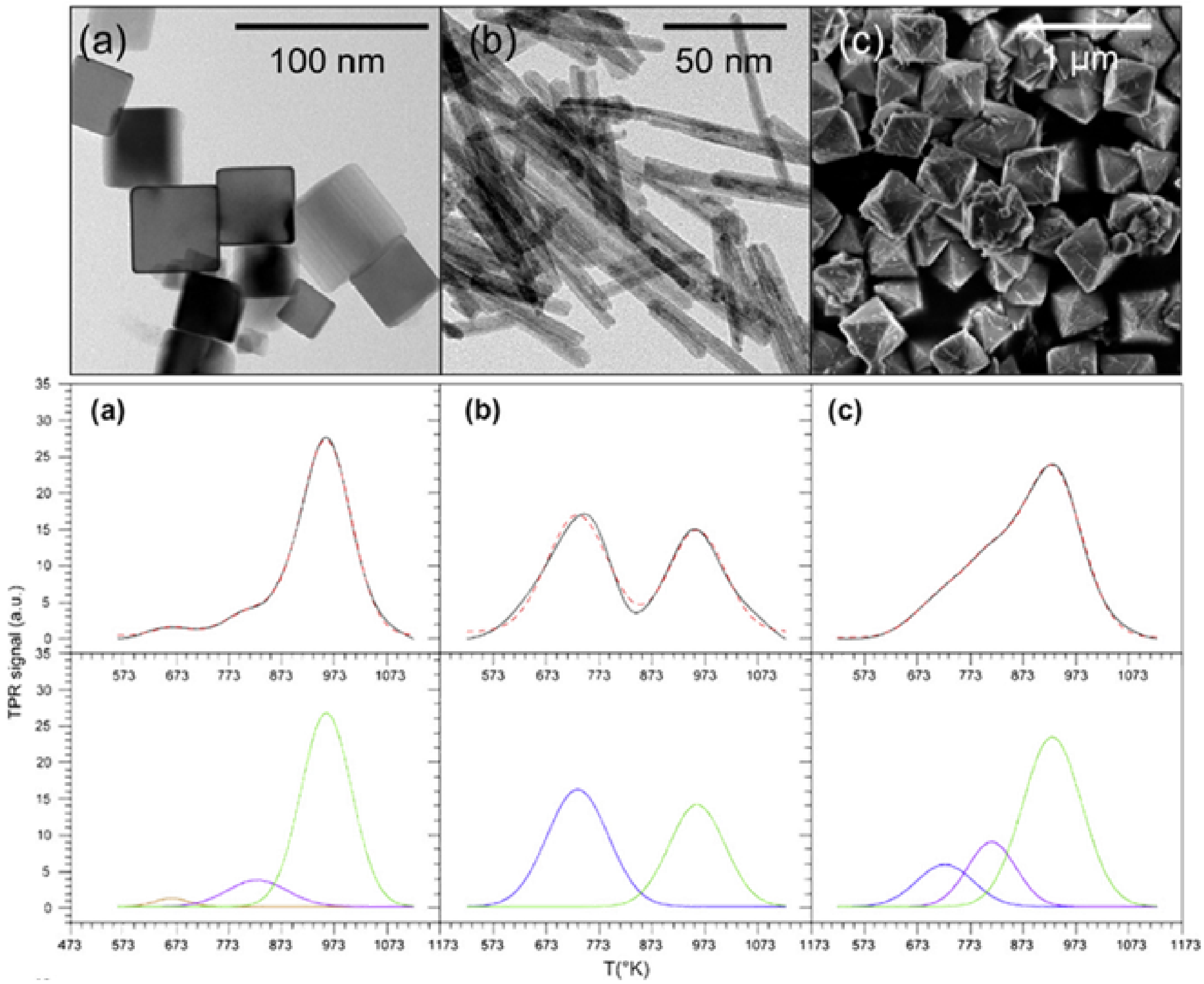

Figure 1: Shape-controlled nano-CeO_2 TEM micrographs and corresponding TPR profiles and deconvolution associated with CeO_2 (a) nanocubes, (b) nanorods, and (c) nanooctahedra. Adapted from Désauney et al. 2013 with permission from Journal of Catalysis.[67]

Analysis of the desorption of H-containing species (using thermal conductivity) from polycrystalline CeO_2 after reduction above 773 K revealed that increasing the reduction temperature decreased the amount of adsorbed H_2.[69] Below 773 K, analysis of the amount of reversibly adsorbed H_2 must be carried out using mass spectrometry, as surface oxygen was susceptible to reduction by the chemisorbed H-containing species, forming water. After reduction above 773 K, only H_2 desorption was observed by mass spectrometry, indicating results from thermal conductivity could be used for analysis. The total H_2 quantity adsorbed per nm^2 CeO_2 increased slightly up to reduction temperatures of 873 K and decreased as the reduction temperature was increased thereafter, even after consideration of particle sintering. These results suggested reduction of the CeO_2 surface was not critical for reversible H_2 adsorption to take place. More recent results, however, do indicate that H_2 can be observed in temperature-programmed experiments monitored by mass spectrometry.[70, 71] This observed H_2 is believed to result from the desorption of H- species that are incorporated into the bulk of CeO_{2-x}, and is directly correlated to the presence of O vacancies, as discussed in the next sections.

2.2 MODIFICATION OF THE CeO_2 BULK BY H_2 TREATMENT

Consumption of H_2 observed in the H_2-TPR of CeO_2 was generally attributed to the reduction of CeO_2 lattice oxygen as discussed above. Yet these studies have also given rise to some important questions: What is the effect of H_2 exposure on the bulk structure of CeO_2? Is there hydrogen incorporation into CeO_2 upon reduction with H_2? Whether H atoms enter the bulk or are merely chemisorbed on the surfaces of CeO_2 is the subject of some debate. Some characterization approaches, described below, suggest incorporation of hydrogen into the bulk of CeO_2 takes place upon high temperature H_2 treatment.

Investigation of CeO_2 during *in situ* reduction in H_2 using X-ray diffraction (XRD) found three zones of lattice behavior.[72, 73] Below 600 K, little change in the CeO_2 lattice takes place. From around 600 – 800 K, a slight expansion in the lattice takes place, followed by a much larger expansion above 850 K. These lattice expansions are consistent with the typical H_2-TPR profiles indicating the observed phenomena are related to reduction of the CeO_2, which could be explained by expansion due to the formation of Ce^{3+} species in the reduced suboxide. It has also been argued that a contribution to this expansion could arise from the incorporation of H into the CeO_2 lattice, potentially in the form of a bronze of the form H_xCeO_2 (or non-stoichiometric cerium oxyhydride). The bronze explanation was originally proposed by Fierro et al.[74] and Cunningham et al.[75] on the basis of ^{1}H nuclear magnetic resonance (^{1}H-NMR) and electron spin resonance (ESR) spectroscopies. Fierro et al. observed the incorporation of H into the CeO_2 sample by ^{1}H-NMR concurrent with the obliteration of bulk ESR signals, which suggested H diffusion into the bulk of the CeO_2 during H_2 treatment up to 673 K. A study by Bekheet et al. found no evidence for incorporation of H in to the CeO_2 lattice by ^{1}H NMR.[58] Matsukawa et al., however, observed the formation of a blue color in a CeO_2 pellet, behavior typical of bronze formation, after brief exposure (30 min) to H_2 at 1073 K in the absence of significant reduction.[76] The formation of the aforementioned blue phase was also accompanied by an expansion of the CeO_2 lattice observed using XRD, consistent with the formation of a H_xCeO_2 bronze phase (x = 0.04 or 0.06). Extended exposure of the sample to the reducing conditions resulted in reduction of the blue proposed bronze to a white CeO_{2-x} suboxide. The role of treatment time in the transient formation of H_xCeO_2 bronzes has not been extensively studied and may explain the aforementioned contradictory NMR results. Bulk and surface hydride species (characterized by vibrational modes from 700-1100 cm^{-1} and 400-600 cm^{-1}, respectively) were also observed by Wu et al. after partial reduction of CeO_2 nanorods by H_2 exposure using inelastic neutron scattering (INS) spectroscopy. This technique is extremely sensitive to hydrogen-containing species, and suggests that hydride species can exist both on the surface and in the bulk of reduced CeO_x.[38] These results agree with a study that observed desorption of H_2 from CeO_2 attributed to H^- incorporated into bulk and surface O vacancy sites.[70] The existence of H-containing species in the CeO_2 lattice under catalytic conditions, however, remains up for debate.

Study of the CeO_2 surface using high-resolution and environmental transmission electron microscopy (TEM) has provided insight into the relationship between H_2 treatment and CeO_2 surface restructuring.[59, 77-80] Oxygen atoms on a CeO_2 (111) surface remained stable under an electron beam,[79] while oxygen atoms on the CeO_2 (100) surface were highly mobile under vacuum conditions (5 x 10^{-6} mbar, CeO_2 nanocubes).[59, 79] Mobility in the (110) surface of the CeO_2 nanocubes was significantly reduced under O_2 and CO_2 environments (5 x 10^{-2}, 2.6 x 10^{-2} mbar, respectively).[59, 79] When the nanocubes were exposed to oxidizing conditions, the CeO_2 nanocube (110) surfaces restructured to form sawtooth CeO_2 (111) nanofacets.[77, 80] Annealing in H_2 ex situ above 773 K prior to observation using TEM resulted in reconstruction of the CeO_2 (110) surface to form larger (111) sawtooth nanofacets.[80] Observation of the reconstruction under environmental TEM conditions (0.7 mbar, up to 1003 K) (see **Figure 2**), however, revealed that H_2 treatment of the (110) surface results in the smoothing of these (111) nanofacets to form a continuous (110) surface, and suggests that this reconstruction is only stable under reducing atmosphere.[77] Further investigation using the same instrument also revealed a reversible partial phase transformation of CeO_2 from the fluorite structure to a C-type Ce_2O_3 structure above 966 K in 0.7 mbar H_2.[78] The phase transformation was completely reversed after cooling below 966 K, and reoxidation of Ce^{3+} to Ce^{4+} was observed, despite cooling in an H_2 environment. Whether this transformation is associated with H incorporation remains unclear.

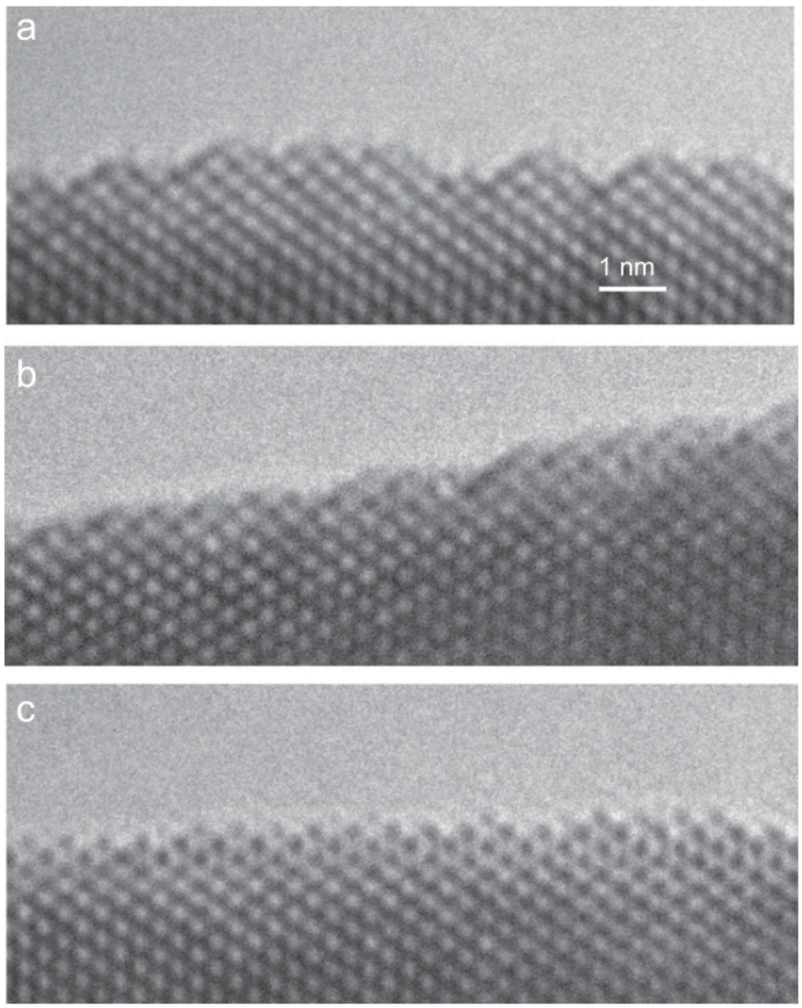

Figure 2: Environmental transmission electron micrographs of a $CeO_2(110)$ surface in 0.7 mbar H_2 at 543 K (a), after heating to 1003 K (b), and during cooling at 873 K (c). The observed $CeO_2(111)$ nanofacets (a) restructured to form a more continuous $CeO_2(110)$ surface (b, c) after treatment at 1003 K in the H_2 atmosphere. Adapted from Crozier et al. 2008 with permission from Ultramicroscopy.[77]

2.3 CHARACTERIZATION OF HYDROGEN SPECIES BY INFRARED AND RAMAN SPECTROSCOPY

A better understanding of the interaction between H_2 and CeO_2 can be achieved using spectroscopic techniques to identify the types of H-containing species on the CeO_2 surface after H_2 exposure. Not all spectroscopic techniques, however, are equal in their ability to detect these H-containing species. While infrared (IR) and Raman spectroscopy have been used to characterize adsorbed OH species, thus far only more H-sensitive techniques such as ^{1}H-NMR and INS have been used successfully to detect small quantities of H in the CeO_2 bulk or Ce-H surface species as discussed earlier.

Infrared spectroscopy has been extensively used to characterize CeO_2 surfaces and their modification after exposure to H_2 or D_2.[8, 22, 26, 38, 47, 48, 81-88] Studies by Lamotte et al. and Binet et al. supported the hypothesis that the coordination of methoxy and OH species occurred via one- (I), two- (II), or three-fold (III) binding through a single oxygen to surface cerium atoms.[81, 82] The appearance of these spectra is shown in **Figure 3**.

Binet et al. observed that after a 673 K pretreatment in O_2 followed by outgassing of CeO_2 with a surface area of 78 m^2 g^{-1}, a mixture of υ(OC) bands consistent with mono- (~1120 cm^{-1}) and bidentate (~1060 cm^{-1}) methoxy species were formed after room-temperature adsorption of methanol, and very little contribution was observed from the tri-dentate species (~1010 cm^{-1}).[8, 82] A shoulder peak in the bidentate region (II', ~1040 cm^{-1}) was assigned to adsorption of the probe molecule near coordinatively unsaturated Ce^{4+} species. As the CeO_2 samples were reduced in H_2 at increasing temperature and subsequently exposed to methanol, the monodentate methoxy species were no longer observed, and a new species was observed at slightly higher wavenumber than the type II bidentate methoxy on O_2-treated CeO_2. This new species was also assigned to a bidentate configuration (II*, ~1080 cm^{-1}), believed to be adsorbed on or near reduced surface sites containing Ce^{3+} (consistent with the formation of surface O vacancies), and became the dominant methoxy species observed after H_2 treatment at temperatures as low as 673 K, consistent with complete surface reduction.[83] An electronic transition, possibly the forbidden $^2F_{5/2} \rightarrow {}^2F_{7/2}$ transition (proposed to no longer be forbidden due to a crystal field effect) or other transitions related to Ce^{3+}, was also assigned to a feature observed at ~ 2120 cm^{-1}.[82]

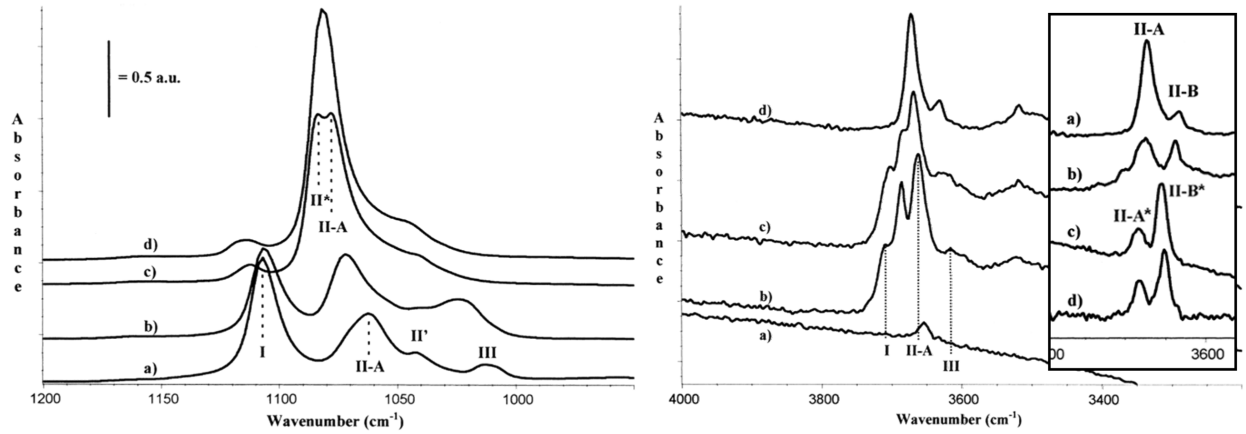

Figure 3: Left: *Spectral features in the υ(OC) region associated with methanol adsorption on CeO_2 after H_2 treatment at (a) 573 K, (b) 623 K, (c) 673 K, and (d) 773 K.* ***Right:*** *Spectral features in the υ(OH) region after (a) O_2 treatment at 873 K, (b) first introduction of 13 kPa H_2 at 573 K, (c) second introduction of 13 kPa H_2 at 573 K, (d) third introduction of 13 kPa H_2 at 573 K.* ***Right Inset:*** *Spectral features in the υ(OH) region after three treatments in 13 kPa H_2 at (a) 573 K, (b) 623 K, (c) 673 K, (d) 773 K. Adapted from Binet et al. 1999 with permission from Catalysis Today.*[8]

When CeO_2 with a surface area of 120 m^2 g^{-1} was subjected to a similar treatment, analogous behavior was observed for surface OH species.[8, 82, 84] After initial oxygen treatment at 673 K, however, υ(OH) bands assigned to bidentate (II-A ~3635 cm^{-1}, II-B ~3654 cm^{-1} analogous to the methoxy II and II’ bands) and hydrogen-bonded (broad, ~3500 cm^{-1}) hydroxyl species were primarily observed, while monodentate species (I, ~3710 cm^{-1}) and tridentate (III, ~3585 cm^{-1}) were less evident.[82] Treatment in O_2 at 873 K was able to remove nearly all the OH species from the CeO_2 surface.[8] Treatment in H_2 at 673 K produced two distinct bidentate species (II*-A, ~3680 cm^{-1}, II*-B, ~3650 cm^{-1}), analogous to methoxy species II* observed after similar treatment over the lower-surface-area CeO_2, and a broad OH stretching feature assigned to hydrogen bonding of residual OH species. Similar distributions of OH species have been observed using Raman spectroscopy, absent from any broad band at ~3520 cm^{-1} associated with H-bonded OH species.[38] When H_2 exposure was performed on CeO_2 pretreated in O_2 at 673 K using small doses of H_2 instead of separate heat treatments, the initially visible II-B υ(OH) band disappeared while the II-A band remained and shifted to higher wavenumber, indicating II-B OH species were more reactive with H_2 than II-A species.[84] The formation of the II*-B OH species was evidently reversible as evacuation at 673 K after H_2 treatment resulted in the disappearance of the II*-B OH species, and subsequent treatment in H_2 caused the species to return.

Adsorption of a range of acidic and basic molecules, summarized by Binet et al., revealed weakly acidic and strongly basic sites on CeO_2 in both its oxidized and reduced state.[8] Results from adsorption of CO_2, dimethyl ether, and pyridine indicated very little difference in acidity resulting from reduction of CeO_2, and peak shifts from pyridine adsorption indicated weaker acid site strength on CeO_2 than ZrO_2 or TiO_2. Similar conclusions could be drawn from adsorption of CO and acetonitrile, which revealed weaker Lewis acidity on the reduced CeO_2 surface.[9] On the other hand, quantification of the base site strength remains a challenge. Adsorption of a proton donor, pyrrole, resulted in dissociation of the probe molecule and could not be used to quantify the base strength of the CeO_2 surface.[88] Low-temperature adsorption of a weaker H-donor, methane, was employed to probe the CeO_2 surface, revealing coordinatively saturated and unsaturated O^{2-} surface species but little about the strength of base sites present on the surface.[89] The adsorption of CO_2, meanwhile, is complex, and while a large amount of CO_2 adsorption occurs, it is difficult to clearly identify and assign individual CO_2 adsorption bands without computational support, especially in polycrystalline samples.[8, 90] Temperature-programmed desorption of CO_2 from shape-controlled nano-CeO_2, however, indicated that nanorods (dominated by (110) and (100) surfaces) contained the highest density of basic sites, followed by nanocubes (predominantly (100) surfaces), then nanooctahedra (predominantly (111) surfaces).[9] The nanoshape surfaces were also probed by $CHCl_3$ and CD_3CN adsorption, indicating a similar trend in base site strength.

Raman spectroscopy has also been used to characterize oxygen defect sites on similar shape-controlled CeO_2 nanoparticles via the presence of different adsorbed O_2 species (superoxide and peroxide) after reduction using H_2, which correspond to different types of oxygen vacancies.[91] Reduction at 673 K results in the formation of both one- and two-electron defects on ceria nanorods (dominated by (110) and (100) surfaces), while the same treatment produces isolated or a mixture of isolated and clustered two-electron defects on CeO_2 nanooctahedra (dominated by (111) surfaces) and nanocubes (dominated by (100) surfaces), respectively. Adsorption of methoxy species on shape-controlled nano-CeO_2 at room temperature found predominantly type I methoxy species on nanorods, while nanocubes contained a majority of a mixture of type I and type II', and nanooctahedra contained very few adsorbed methoxy species (only type I species were detected).[92]

To date, no comparative study exists to demonstrate the difference between OH or methoxy species formed on oxidized and reduced shape-controlled nano-CeO_2.

2.4 HYDROGEN-DEUTERIUM EXCHANGE

The use of H-D exchange has revealed the ability of CeO_2 (and particularly, CeO_2 pre-treated in H_2) to exchange H and D at modest temperatures.[22, 84, 86, 87] When Badri et al. adsorbed D_2 on CeO_2 treated at 673 K in O_2, the formation of υ(OD) bands did not result in any concurrent decrease in observed υ(OH) band intensity until 473 K, indicating that H-D exchange on oxidized CeO_2 did not occur at an appreciable rate until above 423 K.[84] Instead, surface OD species appeared to form in addition to the already present OH species, and converted some of the existing type II-B OH species to type I. The new type II OD species were assigned to type II-A OD species. Further investigation by Werner et al. also found that D_2 dissociation could take place on both stoichiometric CeO_2 and partially reduced CeO_x thin films at pressures above the mbar regime.[22]

When Martin and Duprez measured the rate of H-D exchange using a temperature-programmed isotopic exchange (TPIE) technique, exchange of H and D reached a maximum rate at 433 K over oxidized CeO_2, but when the CeO_2 was treated in H_2 prior to the TPIE, the exchange reached a maximum rate at ~373 K.[87] The apparent activation energies for H-D exchange over the O_2-treated and H_2-treated (723 K) CeO_2 samples were 59 and 26 kJ mol^{-1}, respectively. Evidently the H_2 pretreatment produced a group of more reactive H-containing species on the reduced CeO_2 surface, which caused H-D exchange to take place more rapidly than exchange over other oxides such as ZrO_2 or MgO, and doubled the total quantity of exchanged H. Schimming et al. also measured the apparent activation energy of H-D exchange over CeO_2 pretreated at 723 K in H_2, and found a value of 22 kJ mol^{-1} in agreement with Martin and Duprez.[86] When the exchange was carried out at 423 K, infrared spectroscopy results indicated that type I OH species decreased as type I and II OD species appeared, suggesting exchange of D_2 with type I OH species prior to type II-B OH species. In contrast, Badri et al. observed the formation of type I OH species during their H-D exchange experiments. As Schimming et al. studied the exchange after H_2 pretreatment, while Badri et al. studied the exchange after O_2 pretreatment, it stands to reason that type I OH species are more readily exchanged when the CeO_2 surface is saturated with H-containing species after H_2 pretreatment (including reduction). The H-D exchange measured by Schimming et al. at 623 K was less selective to type I OH species, and instead exchange occurred indiscriminately on all site types.

2.5 STUDIES OVER CERIA THIN FILM

While many studies have focused on the interaction of bulk or polycrystalline CeO_2 with H_2, studies performed under ultra-high vacuum (UHV) offer the possibility of a highly controlled environment to investigate the interaction of H_2 with a well-defined CeO_2 surface. Advances in the growth of bulk-like, ordered $CeO_2(111)$ films with low O-defect contents recently led to studies of pristine and oxygen-deficient $CeO_2(111)$ surfaces after exposure to molecular and atomic hydrogen.[93-95] Investigation of the behavior of CeO_2 under UHV conditions has generated insights into the chemical state and structure of $CeO_2(111)$ surfaces after controlled exposure to these H-containing environments.

Interaction of surface OD species on $CeO_2(111)$ surfaces with atomic D was observed to give rise to D_2O and oxygen vacancies between 150 – 250 K, resulting in a partial reduction of the surface.[96] As the defect density increased to a critical level, D_2O formation was suppressed, at which point D_2 evolution become the more dominant pathway (at ~ 200 – 350 K) for elimination of D from the CeO_2 surface. This behavior may be analogous to the observation of reversible H_2 adsorption on CeO_{2-x} after H_2 pretreatment of a CeO_2 sample,[69] and similarly, to the observation of H_2 evolution behavior correlated to O vacancy density in shape-controlled CeO_2 nanoparticles.[71]When the pristine $CeO_2(111)$ surface was exposed to molecular H_2 at room temperature, no reaction was observed, while exposure to atomic H resulted in a mixture of hydroxyl species and oxygen defects.[57] As should be expected, this result implies that the rate of dissociation of H_2 on $CeO_2(111)$ is negligible under the UHV conditions studied. Later study demonstrated that dissociative adsorption of molecular H_2 could not be observed below pressures of 10 mbar.[22]

Studies using X-ray photoelectron spectroscopy (XPS) to probe the Ce 3d photoemission demonstrated that either the formation of oxygen vacancies or the formation of hydroxyl species can give rise to Ce^{3+} species in the lattice. On reduced $CeO_2(111)$, D_2O could also be irreversibly chemisorbed, causing OD groups to fill anion vacancy sites on the defected surface.[96] Investigation of well-defined $CeO_2(111)$ films under vacuum conditions using nuclear reaction analysis ($^{15}N + {}^{1}H \rightarrow {}^{12}C + \alpha + \gamma$) indicated that thermally reduced, O-defective $CeO_2(111)$ incorporated H species into the bulk of the film after exposure to 10 mbar H_2 at 300 K, while pristine CeO_2 films stabilized H-containing species only at the film surface after the same exposure (see **Figure 4**).[22] These results are consistent with those observed using inelastic neutron scattering spectroscopy, which indicated the formation of bulk Ce-H species after treatment of CeO_2 at 673 K,[38] at which temperature surface reduction (i.e. the formation of vacancies) would be expected. A recent study of H_2 adsorption on pre-reduced ceria (both thin film and nanoparticles) using XPS, electron energy-loss spectroscopy, and ESR suggested that H-containing species exist in Ce^{4+}-H^- pairs, where H^- is stabilized in an O vacancy site, resulting in the re-oxidation of Ce^{3+} species and reforming the atomic structure of the stoichiometric CeO_2.[70]

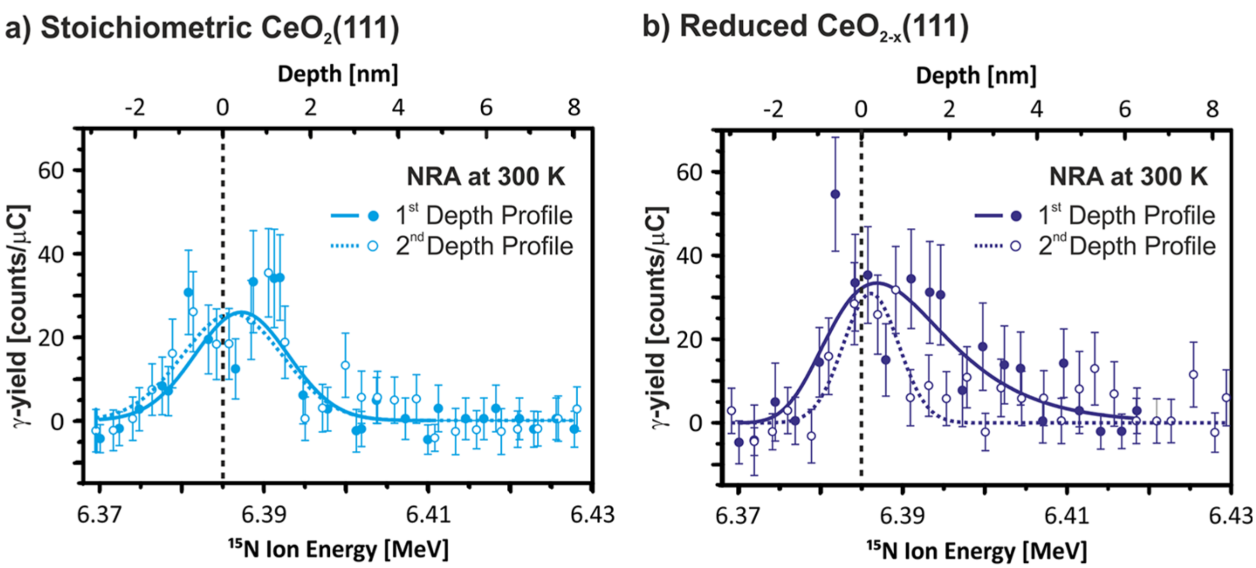

Figure 4: Nuclear reaction analysis depth profiling reveals no evidence of subsurface H species in a) a stoichiometric $CeO_2(111)$ film, but reveals b) the presence of subsurface H species in a $CeO_2(111)$ film pre-treated in 10 mbar H_2 at 300 K. Solid and dotted lines represent trends in the results. Adapted with permission from Werner et al., 2017.[22] Copyright 2017 American Chemical Society.

Conclusions from these studies can be cautiously applied to systems utilizing realistic reaction pressures and treatments. Studies have utilized X-ray photoelectron spectroscopy[22, 57] to determine the oxidation state of H_2-treated CeO_2 particles or surfaces, but care must be taken interpreting these results as partially reduced CeO_2 is sensitive to O_2 exposure, even at low O_2 pressure and typical room temperatures. Furthermore, H_2 treatments performed in UHV systems are often performed at significantly lower pressures than those found in reactors or IR systems, the so-called "pressure gap". As demonstrated by Werner et al., D_2 does not dissociate on $CeO_2(111)$ until pressures well above those typically used in UHV systems, so care must be taken to reproduce experimental work in such controlled environments[22] and the emerging ambient pressure XPS technique may be employed to address this pressure gap.[38]

2.6 Selective Hydrogenation of Alkynes to Alkenes

Hydrogenation of unsaturated C=C and C≡C bonds is well-known to take place over a variety of metal surfaces, especially precious metals such as Pd, which can easily adsorb dissociated H species. Exploration of the ability of metal oxides to perform hydrogenation reactions, however, resulted in the discovery of the ability of CeO_2 to hydrogenate unsaturated C≡C bonds.[26] This unexpected result, and the resulting highly selective hydrogenation behavior, have added significant value to understanding the interaction of H_2 with CeO_2 surfaces and bulk.

Vilé et al. initially reported very high selectivity for the gas-phase hydrogenation of propyne to propene (91% selectivity at 96% conversion) and ethyne to ethene (81% selectivity at 86% conversion) at 523 K in an excess of H_2 (30:1 H_2:alkyne ratio) without significant conversion of the alkene product to alkane. It was noted, however, that increasing the reaction temperature above 523 K resulted in a sharp increase in isomerization products, and increased oligomerization products were observed as catalyst contact times were increased. In contrast to the results from H-D exchange over CeO_2 reported previously, the hydrogenation activity of CeO_2 decreased as the temperature of H_2 pretreatment increased.[25, 26] This result suggests that oxygen vacancies are not favored for hydrogenation over ceria. It remains unclear if the exchangeable H-containing species on the reduced ceria after high-temperature H_2 treatment can be utilized for the selective hydrogenation reaction.

A study of the hydrogenation of a wider range of acetylenic compounds found that CeO_2 supported on TiO_2 is selective for the hydrogenation of the completely unsaturated C≡C bond in the presence of functional groups including olefinic bonds, benzene rings, alcohols, and sulfonates.[32] Results from microcalorimetry of 1-hexyne adsorption on 20% CeO_2 supported on TiO_2 indicated a very large initial heat of adsorption of 900 kJ mol^{-1}, which was ascribed to multiple dehydrogenation steps during adsorption of the 1-hexyne on the clean CeO_2 surface. At higher coverage, the measured adsorption energy was ~200 kJ mol^{-1}, more consistent with a single dehydrogenation step upon chemisorption. Studies using infrared spectroscopy have demonstrated the presence of acetylide species on the CeO_2 surface under reaction conditions,[23, 26] but the relevance of these species to catalysis is not consistent with comparable activity of CeO_2 for the hydrogenation of internal C≡C bonds. Instead, a proposed mechanism for hydrogenation involves π- or di-σ-bonding of the associatively adsorbed C≡C to the active site, where the resulting adsorbate can be easily hydrogenated.[23]

The gas phase (but not liquid phase) hydrogenation rate of acetylenic compounds over these supported CeO_2 catalysts was fairly independent of CeO_2 dispersion, proposed to result from an increase in catalytically inactive surface O-defects (measured using XPS) as the dispersion was increased. Investigation of oriented CeO_2 surfaces for acetylene hydrogenation revealed that the (111) surface of octahedron-like nanoparticles were more active for ethylene hydrogenation at 473 K than nanocubes containing (100) surfaces, which are known to contain higher proportions of O-defected sites.[97] Aging the CeO_2 nanoparticles to produce more (110) surfaces only served to decrease the observed acetylene hydrogenation activity, and was consistent with an inverse relationship between hydrogenation rate and oxygen defect density on the surface of the catalyst (**Figure 5**). While the presence of subsurface H has been reported to play a role in hydrogenation over noble metals in the past,[98] the role of subsurface H species associated with O-defects in ceria remains to be revealed in the hydrogenation reactions.

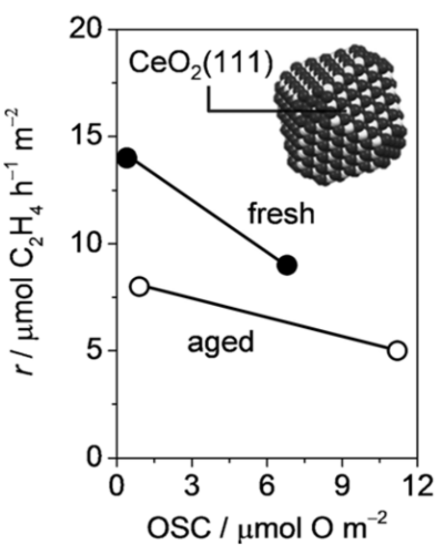

Figure 5: Rate of ethylene formation during ethyne hydrogenation as a function of oxygen storage capacity (OSC) over fresh and aged ceria octahedron-like nanoparticles at 473 K,

indicating an inverse relationship between OSC (proportional to oxygen vacancy density) and hydrogenation rate. Adapted from Vilé et al. 2014, with permission from Angewandte Chemie.[97]

Titania-supported ceria is very stereo-selective to *cis*- isomers of internally unsaturated products (e.g., the hydrogenation of 2-pentyne produced 93% *cis*-2-pentene at 100% conversion) during the hydrogenation of acetylenic compounds.[32] This behavior, and the observation of a parahydrogen-induced polarization (PHIP) effect in the hydrogenation products of alkynes over CeO_2, raises the question of a pairwise H_2-addition mechanism during hydrogenation by oxides.[99] Study of the PHIP effect in hydrogenation reactions over controlled CeO_2 nanoshapes reveals that pairwise addition of H_2 to propylene over CeO_2 is a thermally activated effect, which begins to take place at temperatures above 573 K independent of the CeO_2 facets exposed during hydrogenation of propene.[100] During the hydrogenation of propyne over CeO_2, a significant dependence of the hydrogenation rate on the CeO_2 nanoshape (resulting from variation in the exposed surface) was observed (see **Figure 6**). Nanorods dominated by (110) and (001) surfaces demonstrated a higher pairwise addition selectivity than nanooctahedra dominated by (111) surfaces, which are also known to be the more active surface for the hydrogenation reaction.[101] Nanocubes dominated by (001) surfaces demonstrated a pairwise addition selectivity that was similar to the nanooctahedra, but were less active for the hydrogenation of propylene. This result suggests that the mechanism for H_2 addition is dependent on the exposed surface and is expected to be dominated by a non-pairwise H-addition mechanism over CeO_2 (111) under conditions required to produce high selectivity to the unsaturated hydrogenation product.

Understanding hydrogenation of unsaturated C-C bonds over CeO_2 might provide insights leading to improved selective hydrogenation catalysts. Some studies have suggested the role of so-called "frustrated-Lewis-pairs" (FLPs) consisting of adjacent Ce^{3+} surface species, which lead to a very low barrier for H_2 dissociation and potentially hydrogenation activity.[29, 33] Other studies indicate hydrogenation rates over CeO_2 can be improved by doping other metals into the CeO_2 surface, perhaps modifying these FLPs. Recent studies suggest the potential to improve on hydrogenation activity by doping CeO_2 with Ga to create more hydride species during the dissociation of H_2,[85, 102] while others have directly demonstrated improved hydrogenation rates can be achieved with Ni-doped CeO_2.[27] Further understanding of how these modifications drive faster hydrogenation over CeO_2 might be applied to produce even greater CeO_2-based selective hydrogenation catalysts in the future.

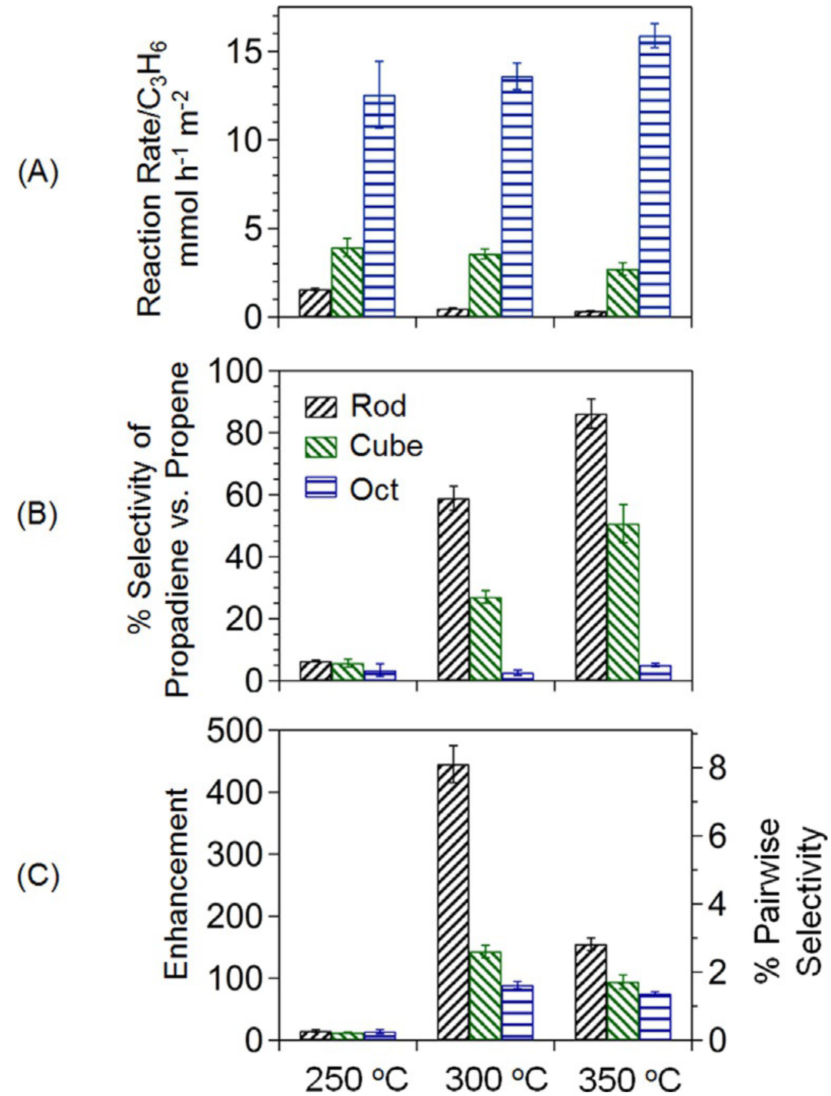

Figure 6: Rate of propylene formation (A), Selectivity towards propadiene vs. propene (B), and ALTADENA NMR signal enhancement (proportional to pairwise selectivity) (C) during propyne hydrogenation over CeO_2 nanoshapes. Adapted from Zhao et al. 2016 with permission from ChemCatChem.[101]

3 COMPUTATIONAL STUDIES

As discussed earlier, ceria itself has demonstrated superior selectivity for selective alkyne hydrogenation. *In situ* techniques (XPS, XAS, DRIFTS, STM) can be combined to obtain fundamental information about ceria-based catalysts under controlled and reaction conditions. However, the hydrogenation mechanism including the dissociation of H_2 and the reaction pathway is still incomplete. In this part, we are going to focus on computational modeling which can give an alternative view of the chemistry taking place over ceria surface and offer inaccessible information on the atomic scale starting from reviewing H_2 interaction, and then the alkyne hydrogenation reactions.

3.1 HYDROGEN INTERACTION ON CERIA SURFACE

Understanding the interaction of hydrogen with ceria is important to develop further insights into different types of hydrogenation reactions. Two H_2 dissociation mechanisms over CeO_2 have been proposed from DFT calculations: homolytic and heterolytic cleavage. Homolytic dissociation of H_2 produces two O-H groups on the surface by binding with two surface oxygen sites, while heterolytic cleavage produces one Ce-H and one O-H species [103]. So far, hydrogen dissociation mechanisms have been proposed based on experimental evidence from infrared spectra that showed O-H and M-H bands for heterolytic and O-H bands for the homolytic cleavage. Hence, heterolytic cleavage has been believed to occur on nonreducible oxide such as MgO [104] or γ-Al_2O_3 [105], while homolytic cleavage has been occurred for reducible oxides such as TiO_2 [106] or CeO_2 [8, 36]. However, García-Melchor et al. [36] demonstrated that polar M-O bond from (111) CeO_2 surface can also cause heterolytic dissociation through DFT calculation using PBE+U method. As shown in **Figure 7**, The homolytic product is thermodynamically stable but heterolytic products are kinetically easier to access. Moreover, the resulting hydride species from heterolytic cleavage can transfer and finally yields the homolytic products. This DFT prediction was later experimentally demonstrated by neutron spectroscopy that hydroxyl groups were observed on oxidized ceria while cerium hydride was present only after oxygen vacancies were created. [38]

Through many studies aimed to understand the H-ceria interaction over a stoichiometric (111) surface, experimental studies suggested that oxygen vacancies play a pivotal role in the reactivity of hydroxyls [96]. Lu et al. [107] and Watkins et al. [108] adapted the surface including oxygen vacancies to investigate the surface reaction with H including H diffusion and H_2O formation. Lu et al. demonstrated that H coupling, surface diffusion and bulk diffusion of H were all promoted at the reduced surface, while H_2O formation was less affected by oxygen vacancies by using on-site Coulomb interaction (DFT+U). On the other hand, Watkins et al. adapted GGA and GGA+U function that incorporated with a local on-site Coulomb repulsion term to cover the questions that whether individual Ce^{4+} ions are reduced or whether electrons are delocalized over many metal ions. This study demonstrated a strongly exothermic character of H_2 chemisorption on the stoichiometric (111) surface and rapid water dissociation were occurred at vacancy sites compared with defect-free ceria surface.

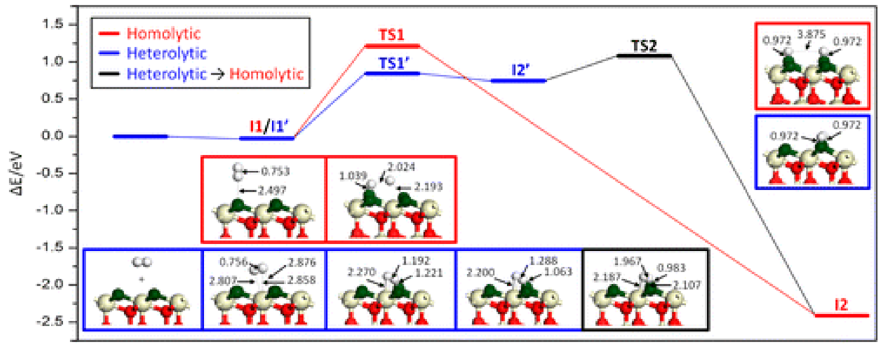

Figure 7. Calculated energy profiles for the homolytic (in red) and heterolytic (in blue) reaction pathways in the H_2 dissociation on CeO_2 (111). The transition state linking the hydrolytic and homolytic products is shown in black. Reprinted from ref [36]. Copyright 2014 American Chemical Society

As we mentioned earlier, not only oxygen vacancies but also different morphologies and crystal planes play an important role in their catalytic reactivity and selectivity. It is noted, however, that extensive modeling studies were focused on (111) facet due to its lowest surface energy and stable structure. Recently, Zhang et al. [109] studied the formation of oxygen vacancies via hydrogen reduction on (111), (110), (100) surfaces to reveal the effect of crystal-planes (see **Figure 8**). The heterolytic dissociation of H_2 was favored over the homolytic dissociation on each surface and, more importantly, (100) surface showed the best performance for H_2 activation. In addition, the role of frustrated Lewis pair over (110) and (100) plane were proposed by the same group regulating the oxygen vacancies [29]. When the oxygen vacancies were created on CeO_2 (110) and (100), two adjacent surface Ce cations proximal to the oxygen vacancy and one neighboring oxygen anion build the FLP sites. The heterolytic cleavage of H_2 is accelerated at FLP sites with a decrease of the activation barrier on CeO_2 (110) and (100) surface, which is attributed to the elongated distance and enhanced acidity and basicity of the Lewis pairs. At the FLP sites, H resource for hydrogenation could originate from hydride at the Ce site which is more active than a proton anchored on an oxygen atom on the surface.

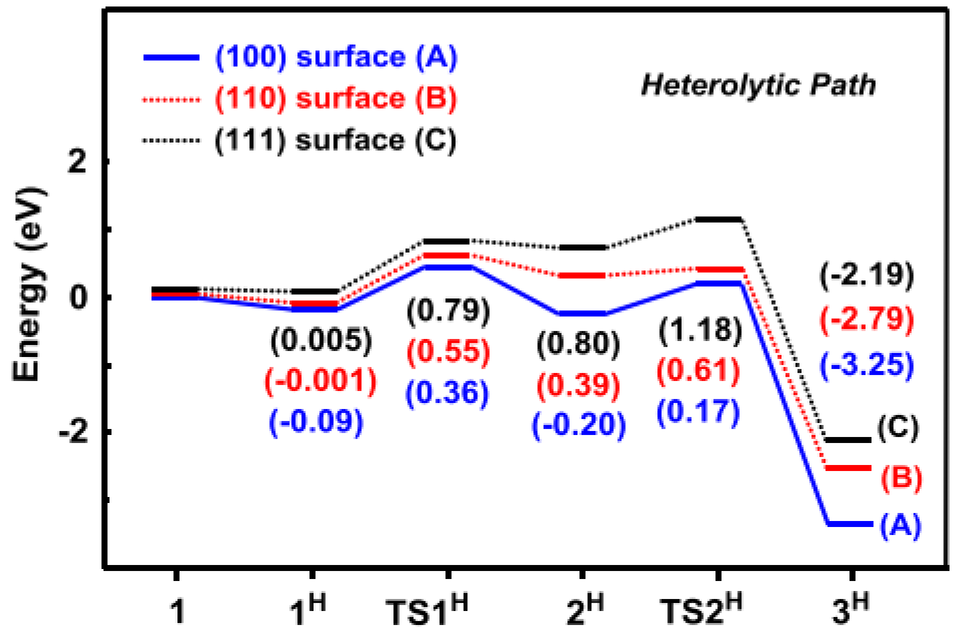

Figure 8. Energy profiles for the heterolytic H_2 dissociation pathways on the (100), (110), and (111) surfaces. Reprinted from ref[109]. Copyright 2019 American Chemical Society

3.2 MECHANISM OF SELECTIVE ALKYNE HYDROGENATION OVER CERIA

A substantial number of DFT studies have been devoted to investigating reaction intermediates and mechanism of alkyne hydrogenation using different approaches and methods. Carrasco et al. [25] studied the acetylene hydrogenation mechanism over CeO_2 (111) with a DFT+U approach. The proposed mechanism was that acetylene adsorption leads to highly active β-C_2H_2 radical species that are hydrogenated to form C_2H_3 with a low energy barrier leading to superior performance for acetylene hydrogenation. Furthermore, the total hydrogenation over CeO_2 (111) from C_2H_5 required a large activation energy barrier which suggests total hydrogenation is an unfavorable reaction. In this study, however, the hydrogen dissociation step was proposed as the rate-limiting step. The intermediate species (β-C_2H_2) formation step is about 4 eV below than the reactant energy and the energy barrier for the final ethylene formation step is about 3 eV, which is kinetically infeasible.

An alternative mechanism, which involved concerted reaction between co-adsorbed H_2 and alkyne, was suggested by García-Melchor et al [36]. This mechanism involved an adsorbed H atom as a hydrogen source for hydrogenation and suggested the formation of oligomers was prevented by restricting the adsorption and diffusion of alkyne molecules over the fully hydroxylated or reduced surface. It was noted, however, that this mechanism also involves a high barrier (~2 eV) and carries a heavy entropic penalty because of the weak adsorption energy of both alkyne and hydrogen species on the surface.

It is noteworthy that the experimental results indicate that the (111) face of CeO_2 is more active than the (110) and (100) faces for acetylene hydrogenation, but there is very little evidence presented to support the importance of oxygen vacancies on the ceria surface in the hydrogenation reaction. Recently, a hydrogenation mechanism over oxygen vacancies of CeO_2 (111) surface was suggested by Riley et al[27]. The proposed mechanism involves the heterolytic dissociation of molecular hydrogen at oxygen vacancies. This causes the exposure of Ce sites followed by Ce-H formation on the surface. The hydride formation prevents the formation of over-stabilized β-C_2H_3 species, and the oxygen vacancy attributes to a decrease in the large kinetic barrier associated with its hydrogenation on the oxygen sites.

Given experimental results and the large formation energy for oxygen vacancy on stoichiometric CeO_2 (111) surface (2.57 eV), the oxygen vacancies are almost certainly involved in hydrogenation, but it is hard to generate oxygen vacancies on a defect-free ceria surface model. A great deal of work has been devoted to examining how the reactivity can be improved by enhancing oxygen vacancy formation. As a result, earlier theoretical works from Nolan [110] and Watson et al. [111] have suggested the doping of divalent ions (e.g. Ni, Cu, Pt, Pd, and Zn) helps to form oxygen vacancies over ceria (111) and (110) surface. The work from Riley et al. [27] also studied the mechanism of acetylene hydrogenation over Ni-doped ceria. It was demonstrated that Ni doping lowered the activation energy barrier of the overall reaction. The doping of divalent metal plays the role of enhancing the formation of oxygen vacancies on ceria surface. It is notable that the Ni dopant was not suggested to directly participate in the hydrogenation reaction but instead to create O-vacancies. In addition to Ni-doped ceria, DFT study for hydrogenation of acetylene over Ga-doped CeO_2 was conducted by Guo et. al [34]. The Ga dopant was shown to promote the formation of surface oxygen vacancies, which create the frustrated Lewis pairs and accelerate heterolytic H_2 cleavage. However, the energy barrier of rate-limiting step in Ga-doped

CeO_2 with higher Ga concentration was 0.21 eV lower than undoped CeO_2 (111), which suggests that Ga is not only working as a promoter to form oxygen vacancy, but also participating in the hydrogenation reaction with the formed Ga-H species.

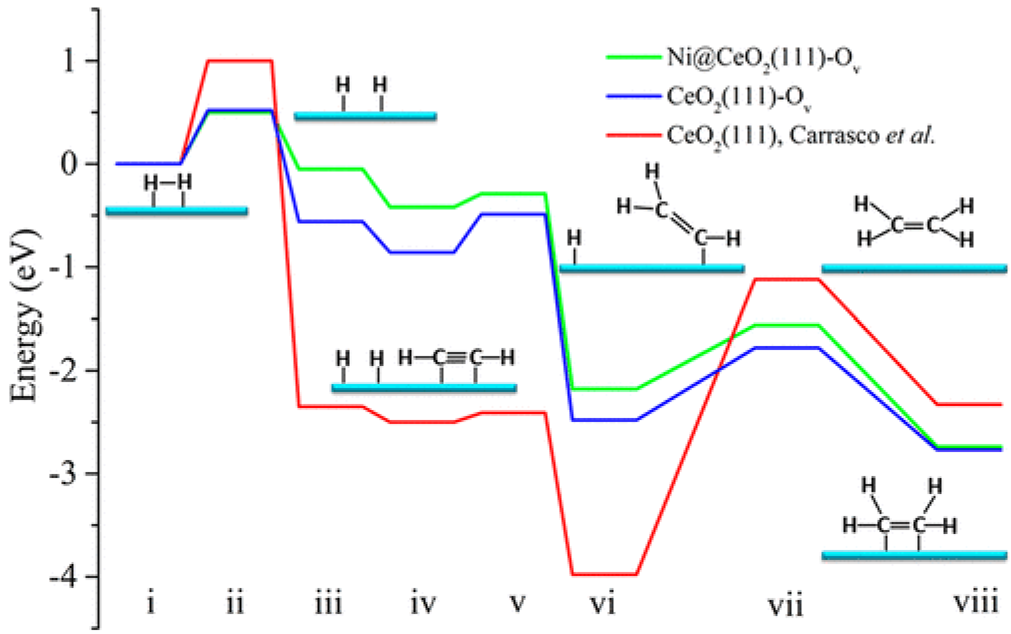

Figure 9 Calculated energy profiles of C_2H_2 hydrogenation on CeO_2(111)-Ov and Ni@CeO_2(111)-Ov with key species illustrated. The results on CeO_2(111) calculated by Carrasco et al. [25] *are also included for comparison. I, H_2*; II, TS1; iii, 2H*; iv, C_2H_2*+2H*; v, TS2; vi, C_2H_3*+H*; vii, TS3; viii, C_2H_4*(energy in the work of Carrasco et al. is for desorbed C_2H_2) here * denotes the adsorption state. Reprinted from ref* [27]*. Copyright 2014 American Chemical Society.*

4 SUMMARY AND OUTLOOK

Ceria-based materials are among the most interesting and widely investigated catalysts, which can be attributed to their excellent redox behavior as well as their versatile acid-base properties. This review surveyed specifically the recently discovered hydrogenation performance of ceria and the fundamental understanding of this unusual property of ceria through both experimental and computational studies. Regarding H_2 adsorption and activation, it is becoming clear that H_2 can dissociate over ceria surface to yield either homolytic (two OHs) or heterolytic products (one OH and one Ce-H) depending on the density of surface O-vacancies. Although the heterolytic dissociation mechanism has a lower activation barrier, the homolytic products are more thermodynamically stable and thus found on stoichiometric ceria surfaces. When used to catalyze alkyne hydrogenation, the reaction was proposed generally limited by the H_2 activation step while the subsequent hydrogenation of adsorbed alkyne species is facile by either the hydride or the hydroxyl species over ceria. As to the role of surface O-vacancies on ceria for the hydrogenation of alkynes, opposing views remain, and more recent computational work supports the active role of surface O-vacancies in activating H_2 and facilitating the hydrogenation pathways. It is expected that continued efforts are needed to further elucidate the reaction mechanisms of selective hydrogenation over ceria and the catalytic role of different hydrogen species as well as O-vacancies.

Despite the interesting hydrogenation performance of ceria, its reaction rate is fairly low, and the reaction temperature is still much higher (> 100 K) than that of typical metal catalysts. To improve the activity and lower the reaction temperature for hydrogenation reactions, further tuning of ceria is certainly needed. Lessons can be learned from the vast number of studies controlling the redox and acid-base properties of ceria as well as the recent investigations of hydrogenation reactions. It is evident that doping of ceria, a large body of work has been done in the past to improve the redox property, is one promising route to enhance the hydrogenation activity of ceria at lower temperatures. The FLPs concept introduced recently in ceria catalysis is certainly interesting and further modification and construction of different types of FLPs via dopants and surface modifications (hybrid systems for example) is expected to lead to more facile H_2 dissociation and hydrogenation steps over ceria. Experimental studies, especially operando studies, and theoretical modeling are paramount for mechanistic understanding of how these modifications of ceria can lead to facile hydrogenation under milder conditions such that practical ceria-based oxides may be designed for hydrogenation catalysis without the use of noble metals.

Acknowledgements

This research was sponsored by the U.S. Department of Energy, Office of Science, Office of Basic Energy Sciences, Chemical Sciences, Geosciences, and Biosciences Division, Catalysis Science program.

REFERENCES

1. Kašpar, J.; Fornasiero, P.; Hickey, N., Automotive catalytic converters: current status and some perspectives. *Catalysis Today* **2003,** *77* (4), 419-449.
2. Yao, H. C.; Yu Yao, Y. F., Ceria in automotive exhaust catalysts I. Oxygen storage. *Journal of Catalysis* **1984,** *86* (2), 254-265.
3. Vivier, L.; Duprez, D., Ceria-Based Solid Catalysts for Organic Chemistry. *ChemSusChem* **2010,** *3* (6), 654-678.
4. Paier, J.; Penschke, C.; Sauer, J., Oxygen Defects and Surface Chemistry of Ceria: Quantum Chemical Studies Compared to Experiment. *Chemical Reviews* **2013,** *113* (6), 3949-3985.
5. Juárez, R.; Concepción, P.; Corma, A.; García, H., Ceria nanoparticles as heterogeneous catalyst for CO2 fixation by ω-aminoalcohols. *Chemical Communications* **2010,** *46* (23), 4181-4183.
6. Leyva-Pérez, A.; Cómbita-Merchán, D.; Cabrero-Antonino, J. R.; Al-Resayes, S. I.; Corma, A., Oxyhalogenation of Activated Arenes with Nanocrystalline Ceria. *ACS Catalysis* **2013,** *3* (2), 250-258.
7. Tamura, M.; Tomishige, K., Redox Properties of CeO2 at Low Temperature: The Direct Synthesis of Imines from Alcohol and Amine. *Angewandte Chemie International Edition* **2015,** *54* (3), 864-867.
8. Binet, C.; Daturi, M.; Lavalley, J. C., IR study of polycrystalline ceria properties in oxidised and reduced states. *Catalysis Today* **1999,** *50* (2), 207-225.
9. Wu, Z.; Mann, A. K. P.; Li, M.; Overbury, S. H., Spectroscopic Investigation of Surface-Dependent Acid–Base Property of Ceria Nanoshapes. *The Journal of Physical Chemistry C* **2015,** *119* (13), 7340-7350.
10. Mann, A. K. P.; Wu, Z.; Calaza, F. C.; Overbury, S. H., Adsorption and Reaction of Acetaldehyde on Shape-Controlled CeO2 Nanocrystals: Elucidation of Structure–Function Relationships. *ACS Catalysis* **2014,** *4* (8), 2437-2448.
11. Wang, Y.; Wang, F.; Song, Q.; Xin, Q.; Xu, S.; Xu, J., Heterogeneous Ceria Catalyst with Water-Tolerant Lewis Acidic Sites for One-Pot Synthesis of 1,3-Diols via Prins Condensation and Hydrolysis Reactions. *Journal of the American Chemical Society* **2013,** *135* (4), 1506-1515.
12. Zhang, S.; Xia, Z.; Zou, Y.; Cao, F.; Liu, Y.; Ma, Y.; Qu, Y., Interfacial Frustrated Lewis Pairs of CeO2 Activate CO2 for Selective Tandem Transformation of Olefins and CO2 into Cyclic Carbonates. *Journal of the American Chemical Society* **2019,** *141* (29), 11353-11357.
13. Zhang, Z.; Wang, Y.; Lu, J.; Zhang, J.; Li, M.; Liu, X.; Wang, F., Pr-Doped CeO2 Catalyst in the Prins Condensation–Hydrolysis Reaction: Are All of the Defect Sites Catalytically Active? *ACS Catalysis* **2018,** *8* (4), 2635-2644.

14. Kaneko, H.; Miura, T.; Ishihara, H.; Taku, S.; Yokoyama, T.; Nakajima, H.; Tamaura, Y., Reactive ceramics of CeO2–MOx (M=Mn, Fe, Ni, Cu) for H2 generation by two-step water splitting using concentrated solar thermal energy. *Energy* **2007,** *32* (5), 656-663.
15. Le Gal, A.; Abanades, S., Dopant Incorporation in Ceria for Enhanced Water-Splitting Activity during Solar Thermochemical Hydrogen Generation. *The Journal of Physical Chemistry C* **2012,** *116* (25), 13516-13523.
16. Mansingh, S.; Padhi, D. K.; Parida, K. M., Enhanced photocatalytic activity of nanostructured Fe doped CeO2 for hydrogen production under visible light irradiation. *International Journal of Hydrogen Energy* **2016,** *41* (32), 14133-14146.
17. Shen, W.-J.; Ichihashi, Y.; Ando, H.; Matsumura, Y.; Okumura, M.; Haruta, M., Effect of reduction temperature on structural properties and CO/CO2 hydrogenation characteristics of a Pd-CeO2 catalyst. *Applied Catalysis A: General* **2001,** *217* (1), 231-239.
18. Trovarelli, A.; Deleitenburg, C.; Dolcetti, G.; Lorca, J. L., CO2 Methanation Under Transient and Steady-State Conditions over Rh/CeO2 and CeO2-Promoted Rh/SiO2: The Role of Surface and Bulk Ceria. *Journal of Catalysis* **1995,** *151* (1), 111-124.
19. Trovarelli, A.; Dolcetti, G.; de Leitenburg, C.; Kaspar, J., CO2 Hydrogenation Over Platinum Group Metals Supported on CeO2: Evidence for a Transient Metal-Support Interaction. In *Studies in Surface Science and Catalysis*, Guczi, L.; Solymosi, F.; TÉTÉNyi, P., Eds. Elsevier: 1993; Vol. 75, pp 2781-2784.
20. Wang, F.; He, S.; Chen, H.; Wang, B.; Zheng, L.; Wei, M.; Evans, D. G.; Duan, X., Active Site Dependent Reaction Mechanism over Ru/CeO2 Catalyst toward CO2 Methanation. *Journal of the American Chemical Society* **2016,** *138* (19), 6298-6305.
21. Kumari, N.; Haider, M. A.; Agarwal, M.; Sinha, N.; Basu, S., Role of Reduced CeO2(110) Surface for CO2 Reduction to CO and Methanol. *The Journal of Physical Chemistry C* **2016,** *120* (30), 16626-16635.
22. Werner, K.; Weng, X.; Calaza, F.; Sterrer, M.; Kropp, T.; Paier, J.; Sauer, J.; Wilde, M.; Fukutani, K.; Shaikhutdinov, S.; Freund, H. J., Toward an Understanding of Selective Alkyne Hydrogenation on Ceria: On the Impact of O Vacancies on H_2 Interaction with CeO_2(111). *J Am Chem Soc* **2017,** *139* (48), 17608-17616.
23. Cao, T.; You, R.; Zhang, X.; Chen, S.; Li, D.; Zhang, Z.; Huang, W., An in situ DRIFTS mechanistic study of CeO_2-catalyzed acetylene semihydrogenation reaction. *Phys Chem Chem Phys* **2018,** *20* (14), 9659-9670.
24. Azizi, Y.; Petit, C.; Pitchon, V., Formation of polymer-grade ethylene by selective hydrogenation of acetylene over Au/CeO2 catalyst. *Journal of Catalysis* **2008,** *256* (2), 338-344.
25. Carrasco, J.; Vilé, G.; Fernández-Torre, D.; Pérez, R.; Pérez-Ramírez, J.; Ganduglia-Pirovano, M. V., Molecular-Level Understanding of CeO2 as a Catalyst for Partial Alkyne Hydrogenation. *The Journal of Physical Chemistry C* **2014,** *118* (10), 5352-5360.
26. Vilé, G.; Bridier, B.; Wichert, J.; Perez-Ramirez, J., Ceria in hydrogenation catalysis: high selectivity in the conversion of alkynes to olefins. *Angew Chem Int Ed Engl* **2012,** *51* (34), 8620-3.
27. Riley, C.; Zhou, S.; Kunwar, D.; De La Riva, A.; Peterson, E.; Payne, R.; Gao, L.; Lin, S.; Guo, H.; Datye, A., Design of Effective Catalysts for Selective Alkyne Hydrogenation by Doping of Ceria with a Single-Atom Promotor. *J Am Chem Soc* **2018,** *140* (40), 12964-12973.
28. Chong, M.; Cheng, D.-g.; Liu, L.; Chen, F.; Zhan, X., Deactivation of CeO2 catalyst in the hydrogenation of benzoic acid to benzaldehyde. *Catalysis Letters* **2007,** *114* (3), 198-201.

29. Zhang, S.; Huang, Z. Q.; Ma, Y.; Gao, W.; Li, J.; Cao, F.; Li, L.; Chang, C. R.; Qu, Y., Solid frustrated-Lewis-pair catalysts constructed by regulations on surface defects of porous nanorods of CeO2. *Nat Commun* **2017,** *8*, 15266.
30. Ma, Y.; Gao, W.; Zhang, Z.; Zhang, S.; Tian, Z.; Liu, Y.; Ho, J. C.; Qu, Y., Regulating the surface of nanoceria and its applications in heterogeneous catalysis. *Surface Science Reports* **2018,** *73* (1), 1-36.
31. Vilé, G.; Albani, D.; Almora-Barrios, N.; López, N.; Pérez-Ramírez, J., Advances in the Design of Nanostructured Catalysts for Selective Hydrogenation. *ChemCatChem* **2016,** *8* (1), 21-33.
32. Vilé, G.; Wrabetz, S.; Floryan, L.; Schuster, M. E.; Girgsdies, F.; Teschner, D.; Pérez-Ramírez, J., Stereo- and Chemoselective Character of Supported CeO_2 Catalysts for Continuous-Flow Three-Phase Alkyne Hydrogenation. *ChemCatChem* **2014,** *6* (7), 1928-1934.
33. Huang, Z.-Q.; Liu, L.-P.; Qi, S.; Zhang, S.; Qu, Y.; Chang, C.-R., Understanding All-Solid Frustrated-Lewis-Pair Sites on CeO2 from Theoretical Perspectives. *ACS Catalysis* **2018,** *8* (1), 546-554.
34. Zhou, S.; Gao, L.; Wei, F.; Lin, S.; Guo, H., On the mechanism of alkyne hydrogenation catalyzed by Ga-doped ceria. *Journal of Catalysis* **2019,** *375*, 410-418.
35. Fernandez-Torre, D.; Carrasco, J.; Ganduglia-Pirovano, M. V.; Perez, R., Hydrogen activation, diffusion, and clustering on CeO_2(111): a DFT+U study. *J Chem Phys* **2014,** *141* (1), 014703.
36. García-Melchor, M.; López, N., Homolytic Products from Heterolytic Paths in H2 Dissociation on Metal Oxides: The Example of CeO2. *The Journal of Physical Chemistry C* **2014,** *118* (20), 10921-10926.
37. García-Melchor, M.; Bellarosa, L.; López, N., Unique Reaction Path in Heterogeneous Catalysis: The Concerted Semi-Hydrogenation of Propyne to Propene on CeO2. *ACS Catalysis* **2014,** *4* (11), 4015-4020.
38. Wu, Z.; Cheng, Y.; Tao, F.; Daemen, L.; Foo, G. S.; Nguyen, L.; Zhang, X.; Beste, A.; Ramirez-Cuesta, A. J., Direct Neutron Spectroscopy Observation of Cerium Hydride Species on a Cerium Oxide Catalyst. *J Am Chem Soc* **2017,** *139* (28), 9721-9727.
39. Mogensen, M.; Sammes, N. M.; Tompsett, G. A., Physical, chemical and electrochemical properties of pure and doped ceria. *Solid State Ionics* **2000,** *129* (1), 63-94.
40. Fan, L.; Wang, C.; Chen, M.; Zhu, B., Recent development of ceria-based (nano)composite materials for low temperature ceramic fuel cells and electrolyte-free fuel cells. *Journal of Power Sources* **2013,** *234*, 154-174.
41. Sun, C.; Li, H.; Chen, L., Nanostructured ceria-based materials: synthesis, properties, and applications. *Energy & Environmental Science* **2012,** *5* (9), 8475-8505.
42. Huang, W.; Gao, Y., Morphology-dependent surface chemistry and catalysis of CeO2 nanocrystals. *Catalysis Science & Technology* **2014,** *4* (11), 3772-3784.
43. Zhang, D.; Du, X.; Shi, L.; Gao, R., Shape-controlled synthesis and catalytic application of ceria nanomaterials. *Dalton Transactions* **2012,** *41* (48), 14455-14475.
44. Trovarelli, A., Catalytic Properties of Ceria and CeO2-Containing Materials. *Catalysis Reviews* **1996,** *38* (4), 439-520.
45. Trovarelli, A.; Llorca, J., Ceria Catalysts at Nanoscale: How Do Crystal Shapes Shape Catalysis? *ACS Catalysis* **2017,** *7* (7), 4716-4735.

46. Polo-Garzon, F.; Bao, Z.; Zhang, X.; Huang, W.; Wu, Z., Surface Reconstructions of Metal Oxides and the Consequences on Catalytic Chemistry. *ACS Catalysis* **2019,** *9* (6), 5692-5707.
47. Daturi, M.; Finocchio, E.; Binet, C.; Lavalley, J. C.; Fally, F.; Perrichon, V., Study of Bulk and Surface Reduction by Hydrogen of $Ce_xZr_{1-x}O_2$ Mixed Oxides Followed by FTIR Spectroscopy and Magnetic Balance. *The Journal of Physical Chemistry B* **1999,** *103* (23), 4884-4891.
48. Daturi, M.; Binet, C.; Lavalley, J.-C.; Galtayries, A.; Sporken, R., Surface investigation on CexZr1-xO2 compounds. *Physical Chemistry Chemical Physics* **1999,** *1* (24), 5717-5724.
49. Qiao, Z.-A.; Wu, Z.; Dai, S., Shape-Controlled Ceria-based Nanostructures for Catalysis Applications. *ChemSusChem* **2013,** *6* (10), 1821-1833.
50. Li, Y.; Shen, W., Morphology-dependent nanocatalysts: Rod-shaped oxides. *Chemical Society Reviews* **2014,** *43* (5), 1543-1574.
51. Chen, S.; Xiong, F.; Huang, W., Surface Chemistry and Catalysis of Oxide Model Catalysts from Single Crystals to Nanocrystals. *Surface Science Reports* **2019**, https://doi.org/10.1016/j.surfrep.2019.100471.
52. Wu, K.; Sun, L.-D.; Yan, C.-H., Recent Progress in Well-Controlled Synthesis of Ceria-Based Nanocatalysts towards Enhanced Catalytic Performance. *Advanced Energy Materials* **2016,** *6* (17), 1600501.
53. Juárez, R.; Parker, S. F.; Concepción, P.; Corma, A.; García, H., Heterolytic and heterotopic dissociation of hydrogen on ceria-supported gold nanoparticles. Combined inelastic neutron scattering and FT-IR spectroscopic study on the nature and reactivity of surface hydrogen species. *Chemical Science* **2010,** *1* (6), 731-738.
54. Schilling, C.; Hofmann, A.; Hess, C.; Ganduglia-Pirovano, M. V., Raman Spectra of Polycrystalline CeO2: A Density Functional Theory Study. *The Journal of Physical Chemistry C* **2017,** *121* (38), 20834-20849.
55. Wang, M.; Wu, X.-P.; Zheng, S.; Zhao, L.; Li, L.; Shen, L.; Gao, Y.; Xue, N.; Guo, X.; Huang, W.; Gan, Z.; Blanc, F.; Yu, Z.; Ke, X.; Ding, W.; Gong, X.-Q.; Grey, C. P.; Peng, L., Identification of different oxygen species in oxide nanostructures with ^{17}O solid-state NMR spectroscopy. *Science Advances* **2015,** *1* (1), e1400133.
56. Zhu, H.-Z.; Lu, Y.-M.; Fan, F.-J.; Yu, S.-H., Selective hydrogenation of nitroaromatics by ceria nanorods. *Nanoscale* **2013,** *5* (16), 7219-7223.
57. Shahed, S. M. F.; Hasegawa, T.; Sainoo, Y.; Watanabe, Y.; Isomura, N.; Beniya, A.; Hirata, H.; Komeda, T., STM and XPS study of CeO2(111) reduction by atomic hydrogen. *Surface Science* **2014,** *628*, 30-35.
58. Bekheet, M. F.; Grunbacher, M.; Schlicker, L.; Gili, A.; Doran, A.; Epping, J. D.; Gurlo, A.; Klotzer, B.; Penner, S., On the structural stability of crystalline ceria phases in undoped and acceptor-doped ceria materials under in situ reduction conditions. *CrystEngComm* **2019,** *21* (1), 145-154.
59. Bugnet, M.; Overbury, S. H.; Wu, Z. L.; Epicier, T., Direct Visualization and Control of Atomic Mobility at {100} Surfaces of Ceria in the Environmental Transmission Electron Microscope. *Nano Letters* **2017,** *17* (12), 7652-7658.
60. Johnson, M.; Mooi, J., Cerium dioxide crystallite sizes by temperature-programmed reduction. *Journal of Catalysis* **1987,** *103* (2), 502-505.

61. Perrichon, V.; Laachir, A.; Bergeret, G.; Fréty, R.; Tournayan, L.; Touret, O., Reduction of cerias with different textures by hydrogen and their reoxidation by oxygen. *J. Chem. Soc., Faraday Trans.* **1994,** *90* (5), 773-781.
62. Bruce, L. A.; Hoang, M.; Hughes, A. E.; Turney, T. W., Surface area control during the synthesis and reduction of high area ceria catalyst supports. *Applied Catalysis A: General* **1996,** *134* (2), 351-362.
63. Giordano, F.; Trovarelli, A.; de Leitenburg, C.; Giona, M., A Model for the Temperature-Programmed Reduction of Low and High Surface Area Ceria. *Journal of Catalysis* **2000,** *193* (2), 273-282.
64. Giordano, F.; Trovarelli, A.; de Leitenburg, C.; Dolcetti, G.; Giona, M., Some Insight into the Effects of Oxygen Diffusion in the Reduction Kinetics of Ceria. *Industrial & Engineering Chemistry Research* **2001,** *40* (22), 4828-4835.
65. Tana; Zhang, M.; Li, J.; Li, H.; Li, Y.; Shen, W., Morphology-dependent redox and catalytic properties of CeO2 nanostructures: Nanowires, nanorods and nanoparticles. *Catalysis Today* **2009,** *148* (1-2), 179-183.
66. Liu, L.; Cao, Y.; Sun, W.; Yao, Z.; Liu, B.; Gao, F.; Dong, L., Morphology and nanosize effects of ceria from different precursors on the activity for NO reduction. *Catalysis Today* **2011,** *175* (1), 48-54.
67. Désaunay, T.; Bonura, G.; Chiodo, V.; Freni, S.; Couzinié, J. P.; Bourgon, J.; Ringuedé, A.; Labat, F.; Adamo, C.; Cassir, M., Surface-dependent oxidation of H_2 on CeO_2 surfaces. *Journal of Catalysis* **2013,** *297*, 193-201.
68. Xu, J.; Harmer, J.; Li, G.; Chapman, T.; Collier, P.; Longworth, S.; Tsang, S. C., Size dependent oxygen buffering capacity of ceria nanocrystals. *Chem Commun (Camb)* **2010,** *46* (11), 1887-9.
69. Bernal, S.; Calvino, J. J.; Cifredo, G. A.; Gatica, J. M.; Omil, J. A. P.; Pintado, J. M., Hydrogen chemisorption on ceria: influence of the oxide surface area and degree of reduction. *Journal of the Chemical Society, Faraday Transactions* **1993,** *89* (18), 3499-3505
70. Li, Z.; Werner, K.; Qian, K.; You, R.; Plucienik, A.; Jia, A.; Wu, L.; Zhang, L.; Pan, H.; Kuhlenbeck, H.; Shaikhutdinov, S.; Huang, W.; Freund, H. J., Oxidation of Reduced Ceria by Incorporation of Hydrogen. *Angew Chem Int Ed Engl* **2019**, https://doi.org/10.1002/anie.201907117.
71. Gao, Y.; Li, R.; Chen, S.; Luo, L.; Cao, T.; Huang, W., Morphology-dependent interplay of reduction behaviors, oxygen vacancies and hydroxyl reactivity of CeO2 nanocrystals. *Phys Chem Chem Phys* **2015,** *17* (47), 31862-71.
72. Lamonier, C.; Wrobel, G.; Bonnelle, J. P., Behaviour of ceria under hydrogen treatment: thermogravimetry and in situ X-ray diffraction study. *Journal of Materials Chemistry* **1994,** *4* (12), 1927-1928.
73. Wrobel, G.; Lamonier, C.; Bennani, A.; D'Huysser, A.; Aboukaïs, A., Effect of incorporation of copper or nickel on hydrogen storage in ceria. Mechanism of reduction. *J. Chem. Soc., Faraday Trans.* **1996,** *92* (11), 2001-2009.
74. Fierro, J. L. G.; Soria, J.; Sanz, J.; Rojo, J. M., Induced changes in ceria by thermal treatments under vacuum or hydrogen. *Journal of Solid State Chemistry* **1987,** *66* (1), 154-162.
75. Cunningham, J.; O'Brien, S.; Sanz, J.; Rojo, J. M.; Soria, J. A.; Fierro, J. L. G., Exceptional susceptibility of ceria-supported rhodium catalyst to inhibitory SMSI effects including acetone hydrogenation. *Journal of Molecular Catalysis* **1990,** *57* (3), 379-396.

76. Matsukawa, T.; Hoshikawa, A.; Niwa, E.; Yashima, M.; Ishigaki, T., Crystal structure of blue-colored ceria during redox reactions in a hydrogen atmosphere. *CrystEngComm* **2018,** *20* (2), 155-158.
77. Crozier, P. A.; Wang, R.; Sharma, R., In situ environmental TEM studies of dynamic changes in cerium-based oxides nanoparticles during redox processes. *Ultramicroscopy* **2008,** *108* (11), 1432-40.
78. Wang, R.; Crozier, P. A.; Sharma, R., Structural Transformation in Ceria Nanoparticles during Redox Processes. *The Journal of Physical Chemistry C* **2009,** *113* (14), 5700-5704.
79. Möbus, G.; Saghi, Z.; Sayle, D. C.; Bhatta, U. M.; Stringfellow, A.; Sayle, T. X. T., Dynamics of Polar Surfaces on Ceria Nanoparticles Observed In Situ with Single-Atom Resolution. *Advanced Functional Materials* **2011,** *21* (11), 1971-1976.
80. Bezkrovnyi, O. S.; Kraszkiewicz, P.; Ptak, M.; Kepinski, L., Thermally induced reconstruction of ceria nanocubes into zigzag {111}-nanofacetted structures and its influence on catalytic activity in CO oxidation. *Catalysis Communications* **2018,** *117*, 94-98.
81. Lamotte, J.; Morávek, V.; Bensitel, M.; Lavalley, J. C., FT-IR study of the structure and reactivity of methoxy species on ThO2 and CeO2. *Reaction Kinetics and Catalysis Letters* **1988,** *36* (1), 113-118.
82. Binet, C.; Badri, A.; Lavalley, J.-C., A Spectroscopic Characterization of the Reduction of Ceria from Electronic Transitions of Intrinsic Point Defects. *The Journal of Physical Chemistry* **1994,** *98* (25), 6392-6398.
83. Badri, A.; Binet, C.; Lavalley, J.-C., Use of methanol as an IR molecular probe to study the surface of polycrystalline ceria. *Journal of the Chemical Society, Faraday Transactions* **1997,** *93* (6), 1159-1168.
84. Badri, A.; Binet, C.; Lavalley, J.-C., An FTIR study of surface ceria hydroxy groups during a redox process with H_2. *Journal of the Chemical Society, Faraday Transactions* **1996,** *92* (23), 4669-4673
85. Vecchietti, J.; Baltanás, M. A.; Gervais, C.; Collins, S. E.; Blanco, G.; Matz, O.; Calatayud, M.; Bonivardi, A., Insights on hydride formation over cerium-gallium mixed oxides: A mechanistic study for efficient H_2 dissociation. *Journal of Catalysis* **2017,** *345*, 258-269.
86. Schimming, S. M.; Foo, G. S.; LaMont, O. D.; Rogers, A. K.; Yung, M. M.; D'Amico, A. D.; Sievers, C., Kinetics of hydrogen activation on ceria–zirconia. *Journal of Catalysis* **2015,** *329*, 335-347.
87. Martin, D.; Duprez, D., Mobility of Surface Species on Oxides. 2. Isotopic Exchange of D_2 with H of SiO_2, Al_2O_3, ZrO_2, MgO, and CeO_2: Activation by Rhodium and Effect of Chlorine. *The Journal of Physical Chemistry B* **1997,** *101* (22), 4428-4436.
88. Binet, C.; Jadi, A.; Lamotte, J.; Lavalley, J. C., Use of pyrrole as an IR spectroscopic molecular probe in a surface basicity study of metal oxides. *Journal of the Chemical Society, Faraday Transactions* **1996,** *92* (1), 123-129.
89. Li, C.; Xin, Q., FT-IR spectroscopic investigation of methane adsorption on cerium oxide. *The Journal of Physical Chemistry* **1992,** *96* (19), 7714-7718.
90. Vayssilov, G. N.; Mihaylov, M.; Petkov, P. S.; Hadjiivanov, K. I.; Neyman, K. M., Reassignment of the Vibrational Spectra of Carbonates, Formates, and Related Surface Species on Ceria: A Combined Density Functional and Infrared Spectroscopy Investigation. *The Journal of Physical Chemistry C* **2011,** *115* (47), 23435-23454.

91. Wu, Z.; Li, M.; Howe, J.; Meyer, H. M., 3rd; Overbury, S. H., Probing defect sites on CeO2 nanocrystals with well-defined surface planes by Raman spectroscopy and O2 adsorption. *Langmuir* **2010,** *26* (21), 16595-606.
92. Wu, Z.; Li, M.; Mullins, D. R.; Overbury, S. H., Probing the Surface Sites of CeO2 Nanocrystals with Well-Defined Surface Planes via Methanol Adsorption and Desorption. *ACS Catalysis* **2012,** *2* (11), 2224-2234.
93. Duchoň, T.; Dvořák, F.; Aulická, M.; Stetsovych, V.; Vorokhta, M.; Mazur, D.; Veltruská, K.; Skála, T.; Mysliveček, J.; Matolínová, I.; Matolín, V., Ordered Phases of Reduced Ceria As Epitaxial Films on Cu(111). *The Journal of Physical Chemistry C* **2013,** *118* (1), 357-365.
94. Duchoň, T.; Dvořák, F.; Aulická, M.; Stetsovych, V.; Vorokhta, M.; Mazur, D.; Veltruská, K.; Skála, T.; Mysliveček, J.; Matolínová, I.; Matolín, V., Comment on "Ordered Phases of Reduced Ceria as Epitaxial Films on Cu(111)". *The Journal of Physical Chemistry C* **2014,** *118* (9), 5058-5059.
95. Barth, C.; Laffon, C.; Olbrich, R.; Ranguis, A.; Parent, P.; Reichling, M., A perfectly stoichiometric and flat CeO2(111) surface on a bulk-like ceria film. *Sci Rep* **2016,** *6*, 21165.
96. Chen, B.; Ma, Y.; Ding, L.; Xu, L.; Wu, Z.; Yuan, Q.; Huang, W., Reactivity of Hydroxyls and Water on a CeO2(111) Thin Film Surface: The Role of Oxygen Vacancy. *The Journal of Physical Chemistry C* **2013,** *117* (11), 5800-5810.
97. Vilé, G.; Colussi, S.; Krumeich, F.; Trovarelli, A.; Perez-Ramirez, J., Opposite face sensitivity of CeO_2 in hydrogenation and oxidation catalysis. *Angew Chem Int Ed Engl* **2014,** *53* (45), 12069-72.
98. Wilde, M.; Fukutani, K.; Ludwig, W.; Brandt, B.; Fischer, J. H.; Schauermann, S.; Freund, H. J., Influence of carbon deposition on the hydrogen distribution in Pd nanoparticles and their reactivity in olefin hydrogenation. *Angew Chem Int Ed Engl* **2008,** *47* (48), 9289-93.
99. Kovtunov, K. V.; Barskiy, D. A.; Salnikov, O. G.; Khudorozhkov, A. K.; Bukhtiyarov, V. I.; Prosvirin, I. P.; Koptyug, I. V., Parahydrogen-induced polarization (PHIP) in heterogeneous hydrogenation over bulk metals and metal oxides. *Chem Commun (Camb)* **2014,** *50* (7), 875-8.
100. Zhao, E. W.; Zheng, H.; Zhou, R.; Hagelin-Weaver, H. E.; Bowers, C. R., Shaped Ceria Nanocrystals Catalyze Efficient and Selective Para-Hydrogen-Enhanced Polarization. *Angew Chem Int Ed Engl* **2015,** *54* (48), 14270-5.
101. Zhao, E. W.; Xin, Y.; Hagelin-Weaver, H. E.; Bowers, C. R., Semihydrogenation of Propyne over Cerium Oxide Nanorods, Nanocubes, and Nano-Octahedra: Facet-Dependent Parahydrogen-Induced Polarization. *ChemCatChem* **2016,** *8* (13), 2197-2201.
102. Vilé, G.; Dähler, P.; Vecchietti, J.; Baltanás, M.; Collins, S.; Calatayud, M.; Bonivardi, A.; Pérez-Ramírez, J., Promoted ceria catalysts for alkyne semi-hydrogenation. *Journal of Catalysis* **2015,** *324*, 69-78.
103. Mas-Ballesté, R.; Lledós, A., 9.27 - H–H Bond Activation. In *Comprehensive Inorganic Chemistry II (Second Edition)*, Reedijk, J.; Poeppelmeier, K., Eds. Elsevier: Amsterdam, 2013; pp 727-766.
104. Gribov, E. N.; Bertarione, S.; Scarano, D.; Lamberti, C.; Spoto, G.; Zecchina, A., Vibrational and Thermodynamic Properties of H2 Adsorbed on MgO in the 300−20 K Interval. *The Journal of Physical Chemistry B* **2004,** *108* (41), 16174-16186.
105. Joubert, J.; Salameh, A.; Krakoviack, V.; Delbecq, F.; Sautet, P.; Copéret, C.; Basset, J. M., Heterolytic Splitting of H2 and CH4 on γ-Alumina as a Structural Probe for Defect Sites. *The Journal of Physical Chemistry B* **2006,** *110* (47), 23944-23950.

106. Menetrey, M.; Markovits, A.; Minot, C., Reactivity of a reduced metal oxide surface: hydrogen, water and carbon monoxide adsorption on oxygen defective rutile TiO_2(110). *Surface Science* **2003,** *524* (1), 49-62.
107. Wu, X.-P.; Gong, X.-Q.; Lu, G., Role of oxygen vacancies in the surface evolution of H at CeO2(111): a charge modification effect. *Physical Chemistry Chemical Physics* **2015,** *17* (5), 3544-3549.
108. Watkins, M. B.; Foster, A. S.; Shluger, A. L., Hydrogen Cycle on CeO_2(111) Surfaces: Density Functional Theory Calculations. *The Journal of Physical Chemistry C* **2007,** *111* (42), 15337-15341.
109. Zhang, W.; Ma, X.-L.; Xiao, H.; Lei, M.; Li, J., Mechanistic Investigations on Thermal Hydrogenation of CO2 to Methanol by Nanostructured CeO2(100): The Crystal-Plane Effect on Catalytic Reactivity. *The Journal of Physical Chemistry C* **2019,** *123* (18), 11763-11771.
110. Nolan, M., Enhanced oxygen vacancy formation in ceria (111) and (110) surfaces doped with divalent cations. *Journal of Materials Chemistry* **2011,** *21* (25), 9160-9168.
111. Kehoe, A. B.; Scanlon, D. O.; Watson, G. W., Role of Lattice Distortions in the Oxygen Storage Capacity of Divalently Doped CeO2. *Chemistry of Materials* **2011,** *23* (20), 4464-4468.

GRAPHICAL ABSTRACT

A Review of Ceria Catalysts for Hydrogenation Reactions

James Kammert, Jisue Moon, Zili Wu*
Chemical Science Division and Center for Nanophase Materials Sciences, Oak Ridge National Laboratory, Oak Ridge, Tennessee 37831, USA

The work overviewed the recently discovered hydrogenation performance of ceria and the fundamental understanding of this unusual property of ceria through both experimental and computational studies on the mechanisms of hydrogen dissociation and alkyne hydrogenation mechanisms.